DO-TH-00/17
November 2000

Parton distributions in the chiral quark model: a continuum computation

Jürgen Baacke[1] and Hendrik Sprenger[2]
Institut für Physik, Universität Dortmund
D - 44221 Dortmund , Germany

Abstract

We compute the parton distributions for the chiral quark model. We present a new technique for performing such computations based on Green functions. This approach avoids a discretization of the spectrum. It therefore does not need any smoothing procedures. The results are similar to those of other groups, however the distributions peak at smaller x.

PACS: 12.38.Lg, 12.39.Ki, 11.15.Pg, 14.20.Dh, 13.60.Hb

[1]e-mail: baacke@physik.uni-dortmund.de
[2]e-mail: sprenger@hal1.physik.uni-dortmund.de

1 Introduction

Nucleon structure functions have been measured since three decades, yielding very precise and detailed information about the parton distributions. Their evolution with Q^2 is one of the important tests of QCD [1] and the predicted asymptotic freedom. There are various phenomenogical ansätze for the form of the parton distribution, which necessarily has to be chosen at some fixed value of Q^2. In principle these functions contain important information on the structure of the nucleon, which in turn should yield information on the dynamics that determines this structure. The problem is that at low Q^2 where one should expect the nucleon to be described by quark model wave functions QCD becomes nonperturbative so that a description by gluons and current quarks is no longer accessible. Rather one expects the system to be described by other effective field degrees of freedom. Among various models which are used to describe the low energy properties like form factors, couplings to the pion and electromagnetic fields or resonance excitations the chiral quark model [2] contains several elements a realistic model should have: there are constituent quarks, there are mesons, the model has chiral symmetry. The nucleon is described as a chiral hedgehog with an occupied valence quarks bound state, as an extension of the Skyrme model. The fact that the model contains quarks, and that the meson field is not elementary, but itself a quark-antiquark condensate, implies that the coupling of the electromagnetic current to the nucleon is described entirely by the quark degrees of freedom. This property makes it a promising issue to compute the nucleon structure functions in this model.

This has been done recently by several groups [3–6]. We do not have anything to add to the general approach and its basic formulae relating the parton distribution to the quark mode functions or the quark Green function in the external field of the chiral hedgehog. We also make a number of technical assumptions which have emerged to be necessary. So the pion field is varied only on the chiral circle, the problem of translation variance remains, and the Pauli-Villars subtraction with a finite cutoff is applied to the quark sea, not to the valence quarks. This is done consistently as well for the self-consistent nucleon solutions as also for the parton distributions [7].

Where we depart from the previous approaches is in the method used for the practical computation of the sea quark distribution functions. All previous approaches start by discretizing the mode spectrum, introducing a large "confining" sphere with appropriate boundary conditions for the quark wave functions. As the spectrum is discrete, the parton distributions are not smooth, and they have to be modified by a smoothing procedure. Though this, and the discretization as such, could introduce some arbitrariness the various groups obtain similar, though slightly different, results.

It has been demonstrated previously that such a discretization can be avoided entirely when computing the energy of the "quark sea". This quantity has been computed by Moussallam [8] using phase shifts, an approach well-known from kink quantization [9]. Alternatively [10] the self energy can be computed from the Euclidian Green function. A self-consistent computation of the hedgehog profile for the nucleon was carried out recently [11]. We will present here a technique for computing the parton distribution in a continuum approach, i.e., without any discretization.

While the self energy can be computed using the Euclidean Green function, by introducing and deforming a suitable integration contour in the complex energy plane, we have to use the Green function in Minkowski space-time if we want to evaluate the parton distribution. So instead of working far from the physical cuts of the Green function, we have

to work on the cut, here. The technique we use is similar to Moussallam' s approach. But of course we compute different physical quantities. So we need more information than just the scattering phase shifts. Furthermore we will make use of the techniques well-known in potential scattering [12] in order to find expressions for the S matrix elements that are suitable both for discussing their analytic properties and regularization, and for numerical computation. Besides avoiding discretization another advantageous feature of our approach is the inclusion of the asymptotic spectrum. Indeed the power behavior of the asymptotic tails of the angular momentum summation and of the momentum integrations is known and these tails can be included on the basis of fits.

The plan of the paper is as follows: In section 2 we introduce the model and the expression which relates the parton distribution to the quark Green function. A short derivation of this relation is given in Appendix A. In section 3 we find analytic expressions for the Green function and for the S matrix, for the case of a bosonic quantum field in an external field. The corresponding expressions for the fermions, used in the real calculation, are given in Appendix B. In Appendix C we derive a relation for the Fourier transform of the Green function, which is the basis for the numerical calculation. The numerical procedure is described in section 4, in section 5 we discuss the results and present our conclusions.

2 The model

The Nambu-Jona-Lasinio (NJL) model is defined by the Lagrangian [13]

$$\mathcal{L}_{\rm NJL} = \bar\psi(i\gamma^\mu\partial_\mu - m)\psi + \frac{G}{2}\left[(\bar\psi\psi)^2 + (\bar\psi i\gamma_5\boldsymbol{\tau}\psi)^2\right] . \tag{2.1}$$

Introducing Lagrange multiplier fields for the scalar and pseudoscalar densities, the action can be written in bosonized form as

$$S_{\rm NJL} = \int d^4x\left\{\bar\psi\Big[i\gamma^\mu\partial_\mu - g\Big(\sigma + i\boldsymbol{\pi}\cdot\boldsymbol{\tau}\gamma_5\Big)\Big]\psi - \frac{\mu^2}{2}\left(\sigma^2+\boldsymbol{\pi}^2\right) + \frac{m\mu^2}{g}\sigma\right\} . \tag{2.2}$$

The parameters of the model are the fermion self-coupling G, the quark mass m. Furthermore, as the model is non-renormalizable, a cutoff Λ has to be introduced. In the bosonized version these parameters appear as the quark-meson coupling g and the symmetry breaking mass parameter μ. They are related to the basic parameters as $g = \mu\sqrt{G}$ and $m\mu^2 = gf_\pi m_\pi^2$. The latter equation expresses μ in terms of physical constants and of the coupling g which remains a free parameter. A further relation is obtained from the gradient expansion of the effective action. The resulting kinetic term of the pion field is normalized correctly if the Pauli-Villars cutoff is fixed as

$$\Lambda = M\sqrt{\exp\left(\frac{4\pi^2}{N_c g^2}\right)} . \tag{2.3}$$

Here M is the "dynamical quark mass" $M = gf_\pi$.

We will not consider the explicit breaking of chiral symmetry by the "current" quark mass m, so we work in the limit $m_\pi = 0$. Furthermore we will restrict the variation of σ and π to the chiral hypersphere

$$\sigma^2 + \boldsymbol{\pi}^2 = f_\pi^2 . \tag{2.4}$$

The the second term in Eq. 2.2 becomes a constant that can be chosen to be zero. In this case, as shown by [14] in proper time regularization, and in [15] in the Pauli-Villars regularization used here, the model admits a solution which can be identified as the nucleon.

The self-consistent nucleon configuration is based on a chiral hedgehog ansatz

$$g\left[\sigma + i\gamma_5 \boldsymbol{\tau}\cdot\boldsymbol{\pi}\right] = M\exp\left\{i\gamma_5\boldsymbol{\tau}\cdot\boldsymbol{\phi}(\mathbf{x})\right\} \equiv \mathbf{M}(\mathbf{x}) \tag{2.5}$$

with

$$\boldsymbol{\phi}(\mathbf{x}) = \hat{\boldsymbol{x}}\vartheta(r) \tag{2.6}$$

for the σ and π fields. In this external field the quark field has a bound state solution identified with the valence quarks. Furthermore the external field leads to a modification of the "sea quark" energy. The self-consistent solution is obtained by minimizing the energy

$$E_{\rm quark} = \frac{1}{\tau}{\rm Tr}\,\log\Big[-i\gamma^\mu\partial_\mu + \mathbf{M}(\mathbf{x})\Big]\,, \tag{2.7}$$

where the trace extends over the negative energy levels as well as over the bound state. It is understood that the vacuum energy is subtracted. Furthermore a Pauli-Villars subtraction using the regulator Λ is required.

We use here profiles $\vartheta(r)$ obtained by us previously [11]. There the sea quark energy was obtained as a trace over Euclidean Green functions.

It has been noticed by several authors that the computation of the parton distributions can be related to the Green function of the quarks in the external field. In contrast to the computation of the energy we have to use the Green function at real energy, not the Euclidean one. This requires some changes with respect to our previous approach, but we will retain its benefits: to avoid working with discrete levels and the corresponding wave functions.

We rederive the expression for the parton distribution in Appendix A, following [3], we obtain for the sea quark contribution

$$\begin{aligned} D_i(x) &= -{\rm Im}\,N_c M_{\rm N}\int\frac{d^4k}{(2\pi)^4}\delta(M_{\rm N}x - k_3 - k_0) \\ &\quad\times\Theta(-k_0 - M){\rm tr}\left[\gamma_0(1+\gamma_0\gamma_3)S_{\rm F}(\mathbf{k},\mathbf{k},k_0)\right]\,. \end{aligned} \tag{2.8}$$

For the antiquarks one has to replace $x\to -x$ and to reverse the sign of the argument on the Θ function. Here and in the following $M_{\rm N}$ denotes the nucleon mass, x is the Bjorken scaling variable, and $S_{\rm F}(\mathbf{k},\mathbf{k},k_0)$ is the Green function of the fermions in the external hedgehog field. It is the Fourier transform of the position space Green function $S_{\rm F}(\mathbf{x},\mathbf{y},t)$ which satisfies

$$\left[i\gamma_\mu\partial_x^\mu - \mathbf{M}(\mathbf{x})\right]S_{\rm F}(\mathbf{x},\mathbf{y},t-t') = \delta(\mathbf{x}-\mathbf{y})\delta(t-t') \tag{2.9}$$

with Feynman boundary conditions. As the external hedgehog field is not translationally invariant it depends on two separate spatial variables, and so does its Fourier transform

$$S_{\rm F}(\mathbf{k},\mathbf{k}',k_0) = \int dt d^3x d^3y e^{i(k_0 t - \mathbf{k}\cdot\mathbf{x} + \mathbf{k}'\cdot\mathbf{y})}S_{\rm F}(\mathbf{x},\mathbf{y},t)\,. \tag{2.10}$$

The relation to the positive and negative energy eigenfunctions U_α, resp., V_α is formally given by

$$\begin{aligned} S_{\rm F}(\mathbf{x},\mathbf{y},t) &= -i\langle T(\psi(\mathbf{x},t)\bar\psi(\mathbf{y},0)\rangle \\ &= i\Theta(t)\sum_{\alpha>0}e^{-iE_\alpha t}U_\alpha(\mathbf{x})\bar U_\alpha(\mathbf{y}) \\ &\quad -i\Theta(-t)\sum_{\alpha<0}e^{i|E_\alpha|t}V_\alpha(\mathbf{x})\bar V_\alpha(\mathbf{y})\,. \end{aligned} \tag{2.11}$$

Here $\alpha > 0$ ($\alpha < 0$) symbolizes the positive (negative) energy states. We will not use this definition for the practical computation, as it would necessitate the discretization of the energy spectrum. Rather the Green function is obtained in terms of mode functions as described in [11].

As usual the Green function $S_{\rm F}$ is written in terms of a bosonic Green function using the ansatz

$$S_{\rm F} = (E + H)G \tag{2.12}$$

where G satisfies

$$\left(H^2 - E^2\right) G(\mathbf{x}, \mathbf{x}', E) = \left[-\Delta + M^2 + \mathcal{V}(\mathbf{x}) - E^2\right] G(\mathbf{x}, \mathbf{x}', E) = -\delta^3(\mathbf{x} - \mathbf{x}') \; . \tag{2.13}$$

Here $\mathcal{V}$ is the potential or vertex operator

$$\mathcal{V}(\mathbf{x}) = i\boldsymbol{\gamma} \cdot \boldsymbol{\nabla}\mathbf{M}(\mathbf{x}) \, . \tag{2.14}$$

$G(\mathbf{x}, \mathbf{x}', E)$ is the inverse of a symmetric operator, it is obtained by standard techniques described in Appendix B.

In addition to the sea quarks the valence quarks contribute to the structure functions. The equation for the $K^P = 0^+$ partial wave is

$$\left[-\Delta + \mathcal{V}^{0^+}(\mathbf{x})\right]\psi_0 = \omega_0^2 \psi_0 \; . \tag{2.15}$$

The spinor ψ_0 is determined by two radial wave functions $h(r)$ and $j(r)$, and the potential $\mathcal{V}^{0+}$ is a 2×2 matrix given in [11]. Defining their Fourier transforms as

$$h(k) = \int_0^\infty dr r^2 j_0(kr) h(r) \; , \tag{2.16}$$

$$j(k) = \int_0^\infty dr r^2 j_1(kr) j(r) \tag{2.17}$$

one finds

$$D_i^{\rm bou}(x) = \frac{N_{\rm c} M_{\rm N}}{\pi} \int_{|M_{\rm N} x - E_{\rm bou}|}^\infty dk \, k \left(h(k)^2 + j(k)^2 - 2 \frac{M_{\rm N} x - E_{\rm bou}}{k} h(k) j(k) \right) \; . \tag{2.18}$$

This expression is equivalent to the bound-state in [3]. The bound state distribution function is convergent.

3 The Green function

We present here an explicit expression for the Green function that can be evaluated without having recurse to discretization, we also derive some further identities that are useful in this context. For the sake of transparency we here consider a scalar field in a spherically symmetric background. The much more involved expressions for fermion fields coupled to the chiral hedgehog are presented in Appendix B.

We consider a scalar field with a space dependent mass term $m(\mathbf{x})$ which for $|\mathbf{x}| \to \infty$ tends to M. We furthermore assume that $m(\mathbf{x})$ only depends on $|\mathbf{x}| = r$ We decompose

$$m^2(\mathbf{x}) = M^2 + \mathcal{V}(r) \; . \tag{3.1}$$

The Green function then obeys the differential equation

$$\left[-E^2 - \Delta + \mathcal{V}(r) + M^2\right] G(\mathbf{x}, \mathbf{x}'; E) = -\delta^3(\mathbf{x} - \mathbf{x}') \; . \tag{3.2}$$

The Fourier transformation of the *free* Green function is given by

$$G^{(0)}(\mathbf{x}, \mathbf{x}'; E) = \int \frac{d^3k}{(2\pi)^3} \frac{e^{i\boldsymbol{k}(\boldsymbol{x}-\boldsymbol{x}')}}{\kappa^2 - k^2 + i\epsilon} \, , \tag{3.3}$$

where $\kappa^2 = E^2 - M^2$. As is well-know the k integration can be carried out and one obtains

$$G^{(0)}(\mathbf{x}, \mathbf{x}'; E) = -\frac{\kappa}{4\pi} \frac{e^{i(\kappa + i\epsilon)R}}{\kappa R} \; , \tag{3.4}$$

with $R = \sqrt{r^2 + r'^2 - 2rr'\cos(\theta)}$. It can be decomposed with respect to Legendre polynomials using the Gegenbauer expansion. One finds

$$\begin{aligned} G^{(0)}(\mathbf{x}, \mathbf{x}'; E) &= \kappa \sum_l \frac{(2l+1)}{4\pi} j_l(\kappa r_<) \Big[y_l(\kappa r_>) - i j_l(\kappa r_>) \Big] P_l(\cos(\theta)) \\ &= -i\kappa \sum_l \frac{(2l+1)}{4\pi} j_l(\kappa r_<) h_l^{(1)}(\kappa r_>) P_l(\cos(\theta)) \; . \end{aligned} \tag{3.5}$$

The spherical Bessel functions are defined as in [16]. The imaginary part is given by

$$\mathrm{Im}\, G^{(0)}(\mathbf{x}, \mathbf{x}'; E) = -\kappa \sum_l \frac{(2l+1)}{4\pi} j_l(\kappa r) j_l(\kappa r') P_l(\cos(\theta)) \; . \tag{3.6}$$

The Green function in the external field is decomposed in an analogous way via

$$G(\mathbf{x}, \mathbf{x}'; E) = -i\kappa \sum_l \frac{(2l+1)}{4\pi} f_l^-(\kappa, r_<) f_l^+(\kappa, r_>) P_l(\cos(\theta)) \; . \tag{3.7}$$

Here the radial mode functions $f_l^\pm$ satisfy the differential equation

$$\left(-\frac{d^2}{dr^2} - \frac{2}{r}\frac{d}{dr} + \frac{l(l+1)}{r^2} - \kappa^2 \right) f_l(\kappa, r) = -\mathcal{V}(r) f_l(\kappa, r) \; . \tag{3.8}$$

The boundary conditions are, in analogy to the spherical Bessel functions:

$$\begin{aligned} \lim_{r\to 0} f^-(\kappa, r)/j_l(\kappa r) &= \text{const.} \, , \\ \lim_{r\to\infty} f^+(\kappa, r)/h_l^{(1)}(\kappa r) &= 1 \; . \end{aligned} \tag{3.9}$$

The normalization of $f_l^-(\kappa, r)$ is determined by the Wronskian

$$r^2 W(f^+, f^-) = f_l^+ \frac{d}{dr} f_l^- - f_l^- \frac{d}{dr} f_l^+ = \frac{-i}{\kappa} \; . \tag{3.10}$$

It is useful for the numerical computation as well as for the separation (subtraction) of the free Green function to split off the Bessel functions via

$$f_l^+(\kappa, r) = \left[1 + c_l^+(\kappa, r)\right] h_l^{(1)}(\kappa r) \, , \tag{3.11}$$

$$f_l^-(\kappa, r) = \left[1 + c_l^-(\kappa, r)\right] j_l(\kappa r) \; . \tag{3.12}$$

The second equation is used only below the first zero of $j_l(\kappa r)$. In fact the function $c_l^-(\kappa, r)$ is pathological as it has poles and zeros at the zeros of j_l and f_l^-, respectively. An alternative, more useful expression for f_l^- is obtained by forming a linear combination of f_l^+ and $(f_l^+)^*$ which becomes regular as $r \to 0$; explicitly

$$\begin{aligned} f_l^-(\kappa, r) &= \frac{1}{2}\Big\{\Big(1 + \bar{c}_l^+(\kappa, r)\Big)\, h_l^{(2)}(\kappa r) \\ &\quad + \frac{1 + \bar{c}_l^+(\kappa, 0)}{1 + c_l^+(\kappa, 0)}\Big(1 + c_l^+(\kappa, r)\Big)\, h_l^{(1)}(\kappa r)\Big\}\,. \end{aligned} \tag{3.13}$$

The function $c_l^+(\kappa, r)$ tends to zero as $r \to \infty$ and goes to a constant as $r \to 0$. It is well suited for numerical computation, using the differential equation obtained by inserting the ansatz (3.11) into Eq. (3.8).

The function c_l^+ is related in a simple way to the S matrix. The relation follows from considering the regular solution f_l^- in the form (3.13). Indeed the S matrix is defined via the asymptotic behavior of the regular solution:

$$\begin{aligned} f_l^-(\kappa, r) &\overset{r\to\infty}{\simeq} \frac{1}{2}\left[h_l^{(2)}(\kappa r) + e^{2i\delta_l(E)} h_l^{(1)}(\kappa r)\right] \\ &= \frac{1}{2}\left[h_l^{(2)}(\kappa r) + \frac{1 + \bar{c}_l^+(\kappa, 0)}{1 + c_l^+(\kappa, 0)} h_l^{(1)}(\kappa r)\right]\,. \end{aligned} \tag{3.14}$$

So the S matrix is given by

$$S_l(E) = e^{2i\delta_l(E)} = \frac{1 + \bar{c}_l^+(\kappa, 0)}{1 + c_l^+(\kappa, 0)}\,. \tag{3.15}$$

As is well-known [9], the phase shift can be used to compute the zero point energy. For the quark sea in the chiral quark model this has been done in [8]; the relation is, in this case,

$$E_0 = -\frac{1}{\pi}\sum_{K^P}(2K+1)\int_0^\infty d\kappa \sqrt{\kappa^2 + M^2}\frac{d\delta_K(\kappa)}{d\kappa}\,. \tag{3.16}$$

For the parton distribution we need the imaginary part of the Green function in momentum space at equal three-momentum. We have

$$\mathrm{Im}\, G(\mathbf{k}, \mathbf{k}, E) = \int d^3x \int d^3x' e^{-i\mathbf{k}(\mathbf{x}-\mathbf{x}')}\frac{1}{2}\left[G(\mathbf{x}, \mathbf{x}', E) - \bar{G}(\mathbf{x}', \mathbf{x}, E)\right]\,. \tag{3.17}$$

As the Green function is a symmetric in its spatial arguments the expression in brackets is just twice the imaginary part of the Green function in position space. It is straightforward to show that this imaginary part is given by

$$\mathrm{Im}\, G(\mathbf{x}, \mathbf{x}', E) = -\kappa \sum_l \frac{(2l+1)}{4\pi} f_l^-(\kappa, r)\bar{f}_l^-(\kappa, r) P_l(\cos\theta)\,. \tag{3.18}$$

This is analogous to the imaginary part of the free Green function (3.6). Moreover the Fourier transform factors in a similar way. If decomposed into partial waves the Fourier transform reduces to a Fourier-Bessel transform and one obtains

$$\mathrm{Im}\, G(\mathbf{k}, \mathbf{k}, E) = -4\pi\kappa \sum_l (2l+1) f_l^-(\kappa, k)\bar{f}_l^-(\kappa, k) \tag{3.19}$$

with

$$f_l^-(\kappa,k) = \int_0^\infty dr\, r^2 f_l^-(\kappa,r) j_l(kr)\ . \tag{3.20}$$

This Fourier transform is problematic as the integral is not absolutely convergent. This problem is analyzed in Appendix C, making use of Wronskian identities for the free and exact Green functions. The final result is

$$\begin{aligned} f_l^-(\kappa,k) &= \left(e^{2i\delta_\kappa}+1\right)\frac{\pi}{4k\kappa}\left\{(-1)^{l+1}\delta(k+\kappa)+\delta(k-\kappa)\right\} \\ &\quad +\frac{\mathcal{P}}{\kappa^2-k^2}\int_0^\infty dr r^2 j_l(kr)\mathcal{V}(r) f_l^-(\kappa,r)\ . \end{aligned} \tag{3.21}$$

Within the range of integration for the parton distribution, Eq. (2.8), the δ functions do not contribute as $k^2-\kappa^2>0$. So in fact only the last term contributes, the integral converges as $\mathcal{V}(r)\to 0$ exponentially as $r\to\infty$. This provides a numerically stable expression for this Fourier transform.

4 Numerical computation

In the main text we have considered scalar fields in order to present the scheme for evaluating the parton distributions on the basis of Green function techniques. We will continue to do so here. Obviously the real computations were done using the formalism based on the Grand spin reduction of the fermion Green function as presented in Appendix B, leading to 4×4 complex coupled differential equations.

The functions $c_l^+(\kappa,r)$ have been calculated by solving the differential equation

$$\left[-\frac{d^2}{dr^2}-2\left(\frac{1}{r}+\kappa\frac{h_l^{(1)\prime}(\kappa r)}{h_l^{(1)}(\kappa r)}\right)\frac{d}{dr}\right] c_l^+(\kappa,r) = -\mathcal{V}(r)\left[1+c_l^+(\kappa,r)\right]\ . \tag{4.1}$$

which follows from Eq. (3.8) by inserting the ansatz (3.11). We have used a simple four-step Runge-Kutta-scheme, the integration was started at values of R much larger than the range of the potential, where c_l^+ vanishes by definition, i.e., by its boundary condition. The accuracy of these solutions was checked by the Wronskian relation, which was constant to at least six significant digits. As a further check we used the unitarity of the S matrix as the 4×4 matrix relation (B.13). This is displayed in Fig. 1

The functions f_l^- where then obtained in the form (3.13). As the Hankel functions become singular at $r=0$ this form is not suitable at very small r. In this region we have used the form (3.12), starting the integration of the differential equation at $r=0$. This solution was normalized correctly by fitting it to the composed solution at some value or r where both solutions are reliable. This is displayed (for one component of the real 4×4 solution) in Fig. 2.

The next step in the computation of $f_l^-(\kappa,k)$, i.e., the the Fourier-Bessel transform, using Eq. (3.21). The Bessel functions were generated recursively, for small r they were obtained via power series expansion. The integrand is then obtained by squaring the Fourier transform and by supplying the pole prefactor $1/(\kappa^2-k^2)^2$. In the fermion case the corresponding operation is given in Eq. (B.14). In this way the integrand is evaluated on a lattice in the variables k and κ. The region of integration is displayed in Fig. 3; the dependence on the scaling variable x comes from the boundary $k\geq k_{\min}=|xM_{\rm N}-k_0|$

with $k_0 = -\sqrt{\kappa^2 + M^2}$ and some simple prefactors, see Eq. (B.19). The first step is the integration over k. As we work with a discrete lattice the lower end of integration could lead to a step structure; this is avoided by fitting the behavior near $k_{\min}$ down to this boundary. The integration over large k is unproblematic, both due to the prefactor $1/(\kappa^2 - k^2)^2$ as to the decrease of the squared Fourier transform.

The next step is the κ integration. Here the lower boundary is $\kappa = 0$ and the integrand is well-behaved there. The behavior at large κ is powerlike, as expected in a loop integration. The integration over the computed integrand was extended to values $\kappa \simeq (25 \div 35)M$, depending on K. The integrand decreases as κ^{-4}, so the integration up to ∞ is appended using an asymptotic tail of the form $A\kappa^{-4} + B\kappa^{-5}$. An example is displayed in Fig. 4. This integration over κ has to be performed at each value of x.

The final step is the summation over Grand spin K and over parity P. The behavior of the terms in this sum is displayed in Fig. 5. We plot the terms for the different parities for the physical quark mass M and for the cutoff mass Λ. The K^{-1} behavior reflects the divergence to be expected from second order perturbation theory. The difference of the quark mass and cutoff is taken in the form [7]

$$D_i^K(x) = D_i^K(x, M) - \frac{M^2}{\Lambda^2} D_i^K(x, \Lambda) \tag{4.2}$$

These terms decrease as K^{-3}. The sum over the K-spin was extended to $K = 18$. The sum over the higher angular momenta was appended using a power fit to the terms computed numerically.

We plot the final results for the isoscalar unpolarized distribution in Figs. 7 and 8. The antiquark distribution is obtained as $\bar{D}_i(x) = -D_i(-x)$

It is interesting to compare these results with second order perturbative contribution

$$\begin{aligned} D_i(x) &= \frac{N_c M_N M^2}{4\pi^2} \int \frac{d^3\mathbf{k}}{(2\pi)^3} \theta(k^3 - |x| M_N) \mathrm{Tr} \left(\tilde{U}(\mathbf{k}) [\tilde{U}(\mathbf{k})]^\dagger \right) \\ &\quad \times \left[\ln \frac{\Lambda^2 + \kappa^2}{M^2 + \kappa^2} - \frac{\kappa^2(\Lambda^2 - M^2)}{(\lambda^2 + \kappa^2)(M^2 + \kappa^2)} \right] \end{aligned} \tag{4.3}$$

with

$$\kappa^2 = \frac{|x| M_N (k^3 - |x| M_N) \mathbf{k}^2}{(k^3)^2} \; . \tag{4.4}$$

This is done for the sum of quark and antiquark distributions in Fig. 6. It is a further numerical cross check to compute the second order perturbative contribution form the mode expansion. This can be done by replacing in the expression for the Fourier transform of the mode function $f_m^{\alpha-}(\kappa, k)$, Eq. (B.15), the exact solution $f_n^{\alpha-}(\kappa, r)$ by the free solution $\delta_n^\alpha j_{K_n}(\kappa r)$. This comparison is included as well in Fig.6. The agreement is not perfect, but it proves the overall consistency and illustrates the precision of our results. As the higher order perturbative contributions, and therefore their error, are less important this graph can be used to improve the overall result by replacing the computed second order by the analytic one.

Finally, it was also checked that the relation

$$\int_0^1 (D_i(x) + D_i(-x)) dx = N_c \tag{4.5}$$

was fulfilled within 0.1%. In principle this relation [3] is valid exactly if the integration is extended to $x = \infty$. As seen in the figures, the integrand is already very small at $x = 1$.

5 Results and Conclusions

We have presented here a new evaluation of the isoscalar nucleon structure functions, using the continuum approach based on the quark Green function in an external background field. This constitutes a natural extension of our use of Green function methods to the computation of self-consistent solutions [11]. The method presents various internal cross checks as mentioned in the previous section. It is a relatively fast method, the computation of the structure function takes about 5 hours on a standard PC with a 450 MHz Pentium processor.

The self-consistent solution was computed using our previous methods. For the quark-meson coupling we have chosen the value $g = 4$ which was found to be preferred by the comparison of the predicted static parameters with experiment. For f_π we have taken the experimental value 93 MeV.

The results for the parton distributions are shown in Figs. 7 and 8. As compared to previous analyses, based on the explicit wave functions of a discretized system, we find an overall agreement as far as order of magnitude and typical structure are concerned. The results are similar to those of Weiss and Goecke [7] and of Wakamatsu and Kubota [5]. There is a tendency, however, of our structure functions to peak at somewhat smaller values of x. In view of some differences in the self-consistent hedgehog profiles and parameters this is however a very satisfactory agreement of entirely different numerical approaches.

Our results are compared to the parton distributions obtained in the GRV parametrisation [17] at $Q^2 = 0.40$ GeV^2, that is, of the order of the cutoff Λ^2. The agreement is certainly qualitative and even semi-quantitative.

One of our main results that our method coroborates previous analyses in a very satisfactory way. However, it also adds a new and efficent tool for such and similar computations. As we have shown it comprises various internal cross checks, some of which are due the use of analytical methods of potential scattering. Furthermore the method is comparatively fast, and so can be useful for more elaborate computations, such as the computation of polarized structure functions [5, 4] and of skewed parton distributions [18]. It would be interesting, furthermore, to study the full Q^2 dependence, as has been done for the bound state contribution by Weigel, Gamberg and Reinhard [19] as well as by Ruiz Arriola [20].

As a side result we have obtained a very fast method for calculating the phase shift. Alternatively to the method employed in [8, 21], the computation of the system of smooth nonoscillating functions $c_n^{\alpha+}$ allows the extraction of the multichannel S matrix. A further possibility - and cross check - is the use of (C.13) and its multichannel extension.

Acknowledgments

H.S. acknowledges the support by the Graduiertenkolleg “Erzeugung und Zerfälle von Elementarteilchen”.

A Parton distribution

The fermion Green function has been formally expressed by the eigenmodes U_α and V_α in Eq. (2.11). Its Fourier transform (2.10) is given by

$$S_F(\mathbf{k},\mathbf{k}',k_0) = -\sum_{\alpha>0}\frac{U_\alpha(\mathbf{k})\bar{U}_\alpha(\mathbf{k}')}{k_0 - E_\alpha + i\epsilon} - \sum_{\alpha<0}\frac{V_\alpha(\mathbf{k})\bar{V}_\alpha(\mathbf{k}')}{k_0 + |E_\alpha| - i\epsilon} \tag{A.1}$$

where the Fourier transform for the eigenspinors is defined via

$$V_\alpha(\mathbf{x}) = \int \frac{d^3k}{(2\pi)^3} V_\alpha(\mathbf{k}) e^{i\mathbf{k}\cdot\mathbf{x}} \tag{A.2}$$

$$U_\alpha(\mathbf{x}) = \int \frac{d^3k}{(2\pi)^3} U_\alpha(\mathbf{k}) e^{i\mathbf{k}\cdot\mathbf{x}} \, . \tag{A.3}$$

The parton distribution of sea quarks is given by [3]

$$q(x) = \frac{N_c M_N}{2\pi}\int d^3X \int_{-\infty}^{\infty} dz^0 e^{ixM_N z^0} \sum_{\alpha<0} e^{i|E_\alpha|z^0} V_\alpha^\dagger(-\mathbf{X})(1+\gamma_0\gamma^3)V_\alpha(-\mathbf{X}-z^0\mathbf{n}_3) \, . \tag{A.4}$$

If one rewrites this in terms of the Fourier transforms, the z^0 and $\mathbf{X}$ integration can be performed with the result

$$q(x) = N_c M_N \int \frac{d^3k}{(2\pi)^3}\sum_{\alpha<0}\delta(|E_\alpha| + xM_N - k^3)\mathrm{tr}\left[(1+\gamma_0\gamma^3)V_\alpha(\mathbf{k})V_\alpha^\dagger(\mathbf{k})\right] \, . \tag{A.5}$$

We note that $1+\gamma_0\gamma^3$ is a hermitean operator. Considering the Green function in the form (A.1) we see that

$$\begin{aligned} &S_F(\mathbf{k},\mathbf{k},k_0)\gamma^0 - \gamma^0 S_F^\dagger(\mathbf{k},\mathbf{k},k_0) \\ &= \sum_{\alpha>0} 2\pi\delta(k^0 - E_\alpha)U_\alpha(\mathbf{k})U_\alpha^\dagger(\mathbf{k}) - \sum_{\alpha<0} 2\pi\delta(k^0+|E_\alpha|)V_\alpha(\mathbf{k})V_\alpha^\dagger(\mathbf{k}) \, . \end{aligned} \tag{A.6}$$

We therefore find

$$q(x) = -\mathrm{Im}\, N_c M_N \int \frac{d^4k}{(2\pi)^4}\delta(xM_N - k^3 - k^0)\Theta(-k^0)\mathrm{tr}\left[(\gamma_0+\gamma^3)S_F(\mathbf{k},\mathbf{k},k^0)\right] \, . \tag{A.7}$$

The restriction of the integration to negative k^0 does not appear in (A.9) of [3]. It does appear in their Eq. (7.3) for the second order perturbative contribution. As is apparent here it is crucial for restricting the integration to the sea quark states. We have remarked below Eq. (3.21) that $\kappa^2 - k^2 > 0$ so that the δ functions do not contribute. In terms of the variables used here

$$k^2 - \kappa^2 = \mathbf{k}^2 - (k^0)^2 + M^2 \geq (k^3)^2 + M^2 - (k^0)^2 = M^2 + x^2M_N^2 - 2xM_N k^0 > 0 \, . \tag{A.8}$$

The antiquark distribution is determined formally by the positive energy eigenspinors. This means that one has to replace the Θ function by $\Theta(k_0)$. At the same time the energy of these levels has to be replaced by $-E_\alpha$, $\alpha > 0$. In the Green function this reversal of sign is obtained by replacing x by $-x$.

B The Green function for the quark system

B.1 The boson Green function

As we have described in section 2 the fermion Green function has been reduced to a bosonic one which satisfies the differential equation (2.13). It is a 8×8 matrix. Using parity it becomes block diagonal with two 4×4 matrices. As the system is invariant with respect to K spin, it can be expanded [22] with respect to K-spin harmonics Ξ_n^{K,K_z} via

$$G(\mathbf{z}, \mathbf{z}', E) = \sum_{K,K_z,P} g_{mn}^{K,P}(r, r', \kappa) \Xi_m^{K,K_z}(\hat{\boldsymbol{z}}) \otimes \Xi_n^{K,K_z\dagger}(\hat{\boldsymbol{z}}') \tag{B.1}$$

with $\kappa = \sqrt{E^2 - M^2}$. The radial Green functions are 4×4 matrices. They can be written in terms of 4 - component mode functions as

$$\begin{aligned} g_{mn}(r, r', \kappa) &= \kappa \Big[\theta(r - r') f_m^{\alpha+}(\kappa, r) f_n^{\alpha-}(\kappa, r') \\ &\quad + \theta(r' - r) f_m^{\alpha-}(\kappa, r) f_n^{\alpha+}(\kappa, r') \Big] \ . \end{aligned} \tag{B.2}$$

The mode functions satisfy the differential equation

$$\left[-\frac{d^2}{dr^2} - \frac{2}{r}\frac{d}{dr} + \frac{K_n(K_n+1)}{r^2} - \kappa^2 \right] f_n^{\alpha}(\kappa, r) = -\mathcal{V}_n^{n'}(r) f_{n'}^{\alpha}(\kappa, r) \ . \tag{B.3}$$

The subscript denotes the four components, the superscript $\alpha = 1 \ldots 4$ labels the four independent solutions which form a fundamental system. The potential $\mathcal{V}_n^{n'}(r)$ is the grand spin partial wave reduction of $\mathcal{V}(\mathbf{x})$, Eq. (2.14). Its explicit form has been given, e.g., in Appendix A of [11].

In order to split off the behavior at $r = 0$ and at $r = \infty$ of the free solutions we write them in the form

$$f_m^{\alpha+}(\kappa, r) = \left[\delta_m^{\alpha} + c_m^{\alpha+}(\kappa, r) \right] h_{K_m}^{(1)}(\kappa r) \ , \tag{B.4}$$

$$f_m^{\alpha-}(\kappa, r) = \left[\delta_m^{\alpha} + c_m^{\alpha-}(\kappa, r) \right] j_{K_m}(\kappa r) \ . \tag{B.5}$$

Here K_m takes the values $K-1, K, K, K+1$ for the four components labelled by m. As for the single component case presented in section 3 the boundary conditions are

$$\lim_{r\to\infty} c_m^{\alpha+}(\kappa, r) = 0 \ , \tag{B.6}$$

$$\lim_{r\to 0} c_m^{\alpha-}(\kappa, r) = \text{const.} \ , \tag{B.7}$$

and the fundamental system $f_m^{\alpha-}$ is fully specified by the Wronskian

$$r^2 W^{\alpha\beta}(f^+, f^-) = f_m^{\alpha+} \frac{d}{dr} f_m^{\beta-} - f_m^{\beta-} \frac{d}{dr} f_m^{\alpha+} = \frac{-i}{\kappa} \delta^{\alpha\beta} \ . \tag{B.8}$$

As for the single-component case $f_n^{\alpha-}$ can be written as

$$\begin{aligned} f_m^{\lambda-}(\kappa, r) &= \frac{1}{2} \Bigg\{ \Big(\delta_{\alpha}^{\lambda} + \bar{c}_{\alpha}^{\lambda+}(\kappa, 0) \Big) \Big[\Big(\delta + c^{+}(\kappa, 0) \Big)^{-1} \Big]_{\gamma}^{\alpha} \Big(\delta_m^{\gamma} + c_m^{\gamma+}(\kappa, r) \Big) h_{K_m}^{(1)}(\kappa r) \\ &\quad + \Big(\delta_m^{\lambda} + \bar{c}_m^{\lambda+}(\kappa, r) \Big) h_{K_m}^{(2)}(\kappa r) \Bigg\} \end{aligned} \tag{B.9}$$

and it was computed in this form except at very small r. The S matrix is defined by the asymptotic behavior of the regular solution $f_m^{\lambda -}(\kappa, r)$, from the representation (B.9) we find

$$S_m^\lambda = \Big(1 + \overline{c}^+(\kappa,0)\Big)_\alpha^\lambda \left(\Big[1 + c^+(\kappa,0)\Big]^{-1}\right)_m^\alpha \ . \tag{B.10}$$

From this form it is not obvious that it is unitary. We have to use the further information that the Green function forms a symmetric matrix

$$g_{mn}(R,R,\kappa) \ = \ g_{nm}(R,R,\kappa) \tag{B.11}$$

which leads to the relation

$$(1+\overline{c}(\kappa,0))_\alpha^n \left[(1+c(\kappa,0))^{-1}\right]_m^\alpha = (1+\overline{c}(\kappa,0))_\alpha^m \left[(1+c(\kappa,0))^{-1}\right]_n^\alpha \ . \tag{B.12}$$

Using this relation one obtains

$$\begin{aligned} S_m^\lambda S^{*\lambda}{}_n &= \Big(1 + \overline{c}^+(\kappa,0)\Big)_\alpha^\lambda \left[\Big(1 + c^+(\kappa,0)\Big)^{-1}\right]_m^\alpha \Big(1 + c^+(\kappa,0)\Big)_\beta^\lambda \left[\Big(1 + \overline{c}^+(\kappa,0)\Big)^{-1}\right]_n^\beta \\ &= \Big(1 + \overline{c}^+(\kappa,0)\Big)_\alpha^\lambda \left[\Big(1 + \overline{c}^+(\kappa,0)\Big)^{-1}\right]_m^\alpha \Big(1 + c^+(\kappa,0)\Big)_\beta^\lambda \left[\Big(1 + c^+(\kappa,0)\Big)^{-1}\right]_n^\beta \\ &= \delta_{mn} \ . \end{aligned} \tag{B.13}$$

This relation can be used to check the numerics. The inaccuracy is less than 10^{-6}. Using the symmetry relation (B.11) in the form (B.12) one can show that the imaginary part of the Green function again factorizes:

$$\mathrm{Im}\, g_{mn}(r,r',\kappa) = -\kappa f_m^{\alpha -}(\kappa,r) f_n^{\alpha -}(\kappa,r') \ . \tag{B.14}$$

For the numerical computation one needs the Fourier transform of the mode functions $f_m^{\alpha -}$. It is given by

$$\begin{aligned} f_m^{\alpha -}(\kappa,k) &= \Big(e^{2i\delta(\kappa)} + 1\Big)_m^\alpha \frac{\pi}{4k\kappa} \delta(k-\kappa) \Big\{(-1)^{m+1}\delta(k+\kappa) + \delta(k-\kappa)\Big\} \\ &\quad + \frac{\mathcal{P}}{\kappa^2 - k^2} \int_0^\infty dr r^2 j_{K_m}(kr) \mathcal{V}_{mn}(r) f_n^{\alpha -}(\kappa, r) \end{aligned} \tag{B.15}$$

where $e^{2i\delta(\kappa)} + 1$ means

$$\Big(e^{2i\delta(\kappa)} + 1\Big)_\lambda^\alpha = S_\lambda^\alpha + \delta_\lambda^\alpha \ . \tag{B.16}$$

With these preparations we can obtain the Green function for the fermion system. We use the Fourier transform of Eq. (2.13):

$$S(\mathbf{k},\mathbf{k},\kappa) \ = \ \Big(-\sqrt{\kappa^2 + M^2} - k\boldsymbol{\alpha}\hat{\boldsymbol{k}} + \gamma_0 M\Big)\, G(\mathbf{k},\mathbf{k},\kappa) \, . \tag{B.17}$$

The action of $\boldsymbol{\alpha}\hat{\boldsymbol{k}}$ onto the spinor harmonics is given by

$$\boldsymbol{\sigma}\hat{\boldsymbol{k}} \begin{pmatrix} \Xi_1(k) \\ \Xi_2(k) \\ \Xi_3(k) \\ \Xi_4(k) \end{pmatrix} \ = \ - \begin{pmatrix} \Xi_2(k) \\ \Xi_1(k) \\ \Xi_4(k) \\ \Xi_3(k) \end{pmatrix} \ . \tag{B.18}$$

Combining the Ξ spinors, the γ matrices and Eq. (B.17) one finds after some algebra

$$\begin{aligned}\int d\Omega_{\mathbf{k}}\,\mathrm{Im\,tr}\,\left[(\gamma_0+\gamma_3)\,S(\mathbf{k},\mathbf{k},\kappa)\right] &= \mathrm{Im}\sum_{K,P}(2K+1)\Big\{\Big(2E-xM_{\mathrm{N}}+M\Big)\Big(g_{11}+g_{44}\Big)\\ &\quad-\Big(2E-xM_{\mathrm{N}}-M\Big)\Big(g_{22}+g_{33}\Big) \qquad\text{(B.19)}\\ &\quad-2(xM_{\mathrm{N}}-E)\frac{E}{k}\Big(g_{12}+g_{34}\Big)+2k\Big(g_{12}+g_{34}\Big)\,.\Big\}\end{aligned}$$

Here we have suppressed labels and arguments of g_{ij}; explicitly they are given by

$$\begin{aligned}\mathrm{Im}\,g_{ij}^{K,P}(k,k,\kappa) &= -\frac{\kappa}{\left(\kappa^2-k^2\right)^2}\int_0^\infty dr r^2 j_{K_i}(kr)\mathcal{V}_{in}(r)f_n^{\alpha-}(\kappa,r)\\ &\quad\times\int_0^\infty dr r^2 j_{K_j}(kr)\mathcal{V}_{jn'}(r)f_{n'}^{*\alpha-}(\kappa,r)\,. \qquad\text{(B.20)}\end{aligned}$$

C Fourier transform

We here discuss the Fourier transform of the mode function $f_l^-(\kappa,r)$

$$f_l^-(\kappa,k)=\int_0^\infty dr\,r^2 f_l^-(\kappa,r)j_l(kr)\,. \qquad\text{(C.1)}$$

This Fourier transform is problematic numerically as the integral is not absolutely convergent.

We start with the differential equations for $f_l^-(\kappa,r)$ given in Eq. (3.8) and for $j_l(kr)$ which reads

$$-\frac{1}{r^2}\frac{d}{dr}r^2\frac{d}{dr}j_l(kr)+\frac{l(l+1)}{r^2}j_l(kr) = k^2 j_l(kr)\,. \qquad\text{(C.2)}$$

From these we derive

$$\begin{aligned}&-\int_0^R dr\left(j_l(kr)\frac{d}{dr}r^2\frac{d}{dr}f_l^-(\kappa,r)-f_l^-(\kappa,r)\frac{d}{dr}r^2\frac{d}{dr}j_l(kr)\right)\\ &+\int_0^R dr r^2 j_l(kr)\mathcal{V}(r)f_l^-(\kappa,r)=\left(\kappa^2-k^2\right)\int_0^R dr r^2 j_l(kr)f_l^-(\kappa,r) \qquad\text{(C.3)}\end{aligned}$$

and after integration by parts

$$\begin{aligned}\int_0^R dr r^2 j_l(kr)f_l^-(\kappa,r) &= \frac{1}{\kappa^2-k^2}\Big\{\int_0^R dr r^2 j_l(kr)\mathcal{V}(r)f_l^-(\kappa,r) \qquad\text{(C.4)}\\ &\quad-R^2\left[j_l(kR)\frac{d}{dR}f_l^-(\kappa,R)-f_l^-(\kappa,R)\frac{d}{dR}j_l(kR)\right]\Big\}\,.\end{aligned}$$

The boundary contribution at $r=0$ vanishes, because both f_l^- and j_l behave as as r^l. The first term on the right hand side is well-defined in the limit $R\to\infty$, due to the decrease of the potential. The two terms in the bracket display an oscillatory behavior with constant amplitude due to the asymptotic behavior of f_l^- :

$$f_l^-(\kappa,r)\simeq f_l^{-,\infty}(\kappa,r)=\frac{1}{2}\left(h_l^{(2)}(\kappa,r)+e^{2i\delta_\kappa}h_l^{(1)}(\kappa,r)\right)\,. \qquad\text{(C.5)}$$

This behavior makes the limit $R \to \infty$ of the integral on the left hand side ill-defined. It is these asymptotic oscillations that we have to split off.

Using the Wronski determinants for the free Bessel functions and Eq. (C.4) one finds

$$\begin{aligned}
&\int_0^R dr r^2 j_l(kr) \left(f_l^-(\kappa, r) - f_l^{-,\infty}(\kappa, r) \right) \\
&= \frac{1}{\kappa^2 - k^2} \Bigg\{ \int_0^R dr r^2 j_l(kr) \mathcal{V}(r) f_l^-(\kappa, r) \\
&- R^2 \Big[j_l(kR) \frac{d}{dR} \left(f_l^-(\kappa, R) - f_l^{-,\infty}(\kappa, R) \right) \\
&- \left(f_l^-(\kappa, R) - f_l^{-,\infty}(\kappa, R) \right) \frac{d}{dR} j_l(kR) \Big] - i \frac{k^l}{2\kappa^{l+1}} \left(e^{2i\delta_\kappa} - 1 \right) \Bigg\} . \qquad \text{(C.6)}
\end{aligned}$$

The limit $R \to \infty$ of this equation is well-defined. One obtains

$$\begin{aligned}
\int_0^\infty dr r^2 j_l(kr) \left(f_l^+(\kappa, r) - f_l^{-,\infty}(\kappa, r) \right) &= \frac{1}{\kappa^2 - k^2} \Big[\int_0^\infty dr r^2 j_l(kr) \mathcal{V}(r) f_l^-(\kappa, r) \\
&\quad - i \frac{k^l}{2\kappa^{l+1}} \left(e^{2i\delta_\kappa} - 1 \right) \Big] . \qquad \text{(C.7)}
\end{aligned}$$

Both parts of the integral on the left hand side are still ill-defined.

In scattering theory this problem is solved by working with normalizable wave functions obtained by giving small imaginary parts to the momenta (here κ) and taking the appropriate limit to the real axis. This is of course the origin of the physical cuts. This is usually done using Jost functions [12], like $f_l^+(\kappa, r)$, which asymptotically behave as $\exp(\pm i\kappa r)$. However, for brevity of presentation, we have preferred to work here with f_l^- directly. The following results are a heuristic presentation of what we have obtained by using the meticulous $i\epsilon$ prescriptions.

The Fourier transforms of the free solutions $h_l^{(1)}(\kappa r) = j_l(\kappa r) + i y_l(\kappa r)$ are[3]

$$\int_0^\infty dr r^2 j_l(kr) j_l(\kappa r) = \frac{\pi}{2k\kappa} \left\{ (-1)^{l+1} \delta(k + \kappa) + \delta(k - \kappa) \right\} . \qquad \text{(C.8)}$$

and

$$\int_0^\infty dr r^2 j_l(kr) y_l(\kappa r) = k^l \frac{\mathcal{P}}{(\kappa^2 - k^2)\kappa^{l+1}} . \qquad \text{(C.9)}$$

One obtains

$$\begin{aligned}
f_l^-(\kappa, k) &= \left(e^{2i\delta_\kappa} + 1 \right) \frac{\pi}{4k\kappa} \left\{ (-1)^{l+1} \delta(k + \kappa) + \delta(k - \kappa) \right\} \\
&\quad + \frac{\mathcal{P}}{\kappa^2 - k^2} \int_0^\infty dr r^2 j_l(kr) \mathcal{V}(r) f_l^-(\kappa, r) .
\end{aligned}$$

As we have mentioned in the main text, the distribution character of this result does not play a role in the numerical computation. The finite integral which appears on the right hand side plays a central role in evaluating the parton distributions. Using further the methods of potential scattering we can derive a useful identity relating this integral to the S matrix.

[3] $\mathcal{P}$ means principle value

The integral equation accompanying the differential equation (3.8) for the solutions f^+ reads

$$\begin{aligned} f_l^+(\kappa,r) &= -i\kappa\int_0^r dr' r'^2 j_l(\kappa r') h_l^{(1)}(\kappa r)\mathcal{V}(r') f_l^+(\kappa,r') \\ &\quad -i\kappa\int_r^\infty dr' r'^2 j_l(\kappa r) h_l^{(1)}(\kappa r')\mathcal{V}(r') f_l^+(\kappa,r') \ . \end{aligned} \tag{C.10}$$

As asymptotically $f_l^+(\kappa,r)$ behaves as $h_l^{(1)}(\kappa r)$ one finds

$$\frac{i}{\kappa} = \int_0^\infty dr' r'^2 j_l(\kappa r')\mathcal{V}(r') f_l^+(\kappa,r') \ . \tag{C.11}$$

Combining f^- using f^+ in the usual form

$$f_l^-(\kappa,r) = \frac{1}{2}\left(f^{*+}_l(\kappa,r) + e^{2i\delta_\kappa} f_l^+(\kappa,r)\right) \tag{C.12}$$

the integral takes for $k=\kappa$ the form

$$\int_0^\infty dr r^2 j_l(\kappa r)\mathcal{V}(r) f_l^-(\kappa,r) = \frac{i}{2\kappa}\left(e^{2i\delta_\kappa}-1\right) \ . \tag{C.13}$$

This relation has been used as a useful crosscheck. A further cross check is obtained form the Born approximation to this relation:

$$-\kappa\int_0^\infty dr\, r^2 j_l^2(\kappa r)\mathcal{V}(r) = \delta_l^{(1)}(\kappa) \tag{C.14}$$

which determines the behavior of the phase shifts at large l and at large κ.

References

[1] E. Reya, *Phys. Rept.* **69**, 195 (1981).

[2] For recent reviews see: R. Alkofer, H. Reinhardt, and H. Weigel, Phys. Rept. **265**, 139 (1996), hep-ph/9501213; Christov et al., Prog. Part. Nucl. Phys. **A5**, 1 (1996), hep-ph/9604441; D. Diakonov and V. Y. Petrov, hep-ph/0009006.

[3] D. Diakonov, V. Petrov, P. Pobylitsa, M. Polyakov, and C. Weiss, *Nucl. Phys.* **B480**, 341 (1996), hep-ph/9606314.

[4] D. Diakonov, V. Petrov, P. Pobylitsa, M. Polyakov, and C. Weiss, Phys. Rev. **D56**, 4069 (1997), hep-ph/9703420.

[5] M. Wakamatsu and T. Kubota, Phys. Rev. **D57**, 5755 (1998), hep-ph/9707500; M. Wakamatsu and T. Kubota, Phys. Rev. **D60**, 034020 (1999), hep-ph/9809443.

[6] H. Weigel, L. Gamberg, and H. Reinhardt, *Mod. Phys. Lett.* **A11**, 3021 (1996)

[7] C. Weiss and K. Goeke, hep-ph/9712447.

[8] B. Moussallam, *Phys. Rev.* **D40** 3430 (1989).

[9] R. Rajaraman, *Solitons and Instantons* Chapter 5.4, North-Holland, Amsterdam (1989).

[10] J. Baacke, *Z. Phys.* **C47**, 263 (1990); *ibid.*619 (1990).

[11] J. Baacke and H. Sprenger, *Phys. Rev.* **D60**, 05401 (1999), hep-ph/9809428.

[12] V. de Alfaro and T. Regge, *Potential scattering*, North-Holland, Amsterdam (1965)

[13] Y. Nambu and G. Jona-Lasinio, *Phys. Rev.* **122**, 345 (1961); *ibid.* **124**, 246 (1961).

[14] H. Reinhardt and R. Wunsch, Phys. Lett. **B215**, 577 (1988).

[15] F. Döring, A. Blotz, C. Schüren, T. Meissner, E. Ruiz-Arriola and K. Goeke, Nucl. Phys. **A536**, 548 (1992).

[16] M. Abramowitz and I. Stegun, *Handbook of mathematical functions*, Dover publication, New York (1972).

[17] M. Glück, E. Reya, and A. Vogt, Z. Phys. **C67**, 433 (1995).

[18] V. Y. Petrov, P. V. Pobylitsa, M. V. Polyakov, I. Bornig, K. Goeke and C. Weiss, Phys. Rev. **D57**, 4325 (1998), hep-ph/9710270.

[19] H. Weigel, L. Gamberg and H. Reinhardt, Phys. Rev. **D55**, 6910 (1997) hep-ph/9609226.

[20] E. Ruiz Arriola, Nucl. Phys. **A641**, 461 (1998).

[21] E. Farhi, N. Graham, R. L. Jaffe and H. Weigel, Nucl. Phys. **B585**, 443 (2000), hep-th/0003144.

[22] S. Kahana and G. Ripka, Nucl. Phys. **A429**, 462 (1984).

Figure captions

Figure 1: Unitarity of S matrix: $(S^\dagger S)^1_1(\kappa)$ for $K^P = 1^+$: solid line: total matrix element, other lines: the eight components $S_1^{*a} S_1^a$, $a = 1 \ldots 4$, product of real parts and product of imaginary parts.

Figure 2: Behavior of $f_1^{1-}(\kappa, r)$ for ($K^P = 5^+$, $\kappa = 1$), at small r. dashed line: computed via Eq. (3.13), long dashed line: computed via Eq. (3.12).

Figure 3: Integration area in a $k - \kappa$ plane: the dashed line represents position of the pole, the lower solid line is the minimal lower limit of the integration, the upper solid line shows the lower limit for a positive value of x.

Figure 4: Convergence of the κ integration: integrand for the mode function at $x = .25$ for $K^P = 5^+$; solid line: the integrand, dashed line: power fit with $A\kappa^{-4} + B\kappa^{-5}$.

Figure 5: Behavior of Grand spin contributions to $D_i(x = .25)$ at large values of K: solid and dashed lines: parities + and − with dynamical mass; dotted and long-dashed lines: parities + and − with cutoff mass; dash-dotted lines: regulated contribution.

Figure 6: Second order contribution; solid line: computed via a Feynman graphs; dashed line: computed via second order mode sum.

Figure 7: The isosinglet unpolarized distribution of quarks and antiquarks $\frac{1}{2}[q(x) + \bar{q}(x)]$ solid line: total result, dotted line: valence contribution, dashed line: sea contribution, squares: NLO GRV [17] parametrisation

Figure 8: The isosinglet unpolarized distribution of quarks and antiquarks $\frac{1}{2}[q(x) - \bar{q}(x)]$ solid line: total result, dashed line: sea contribution, squares: NLO GRV [17] parametrisation

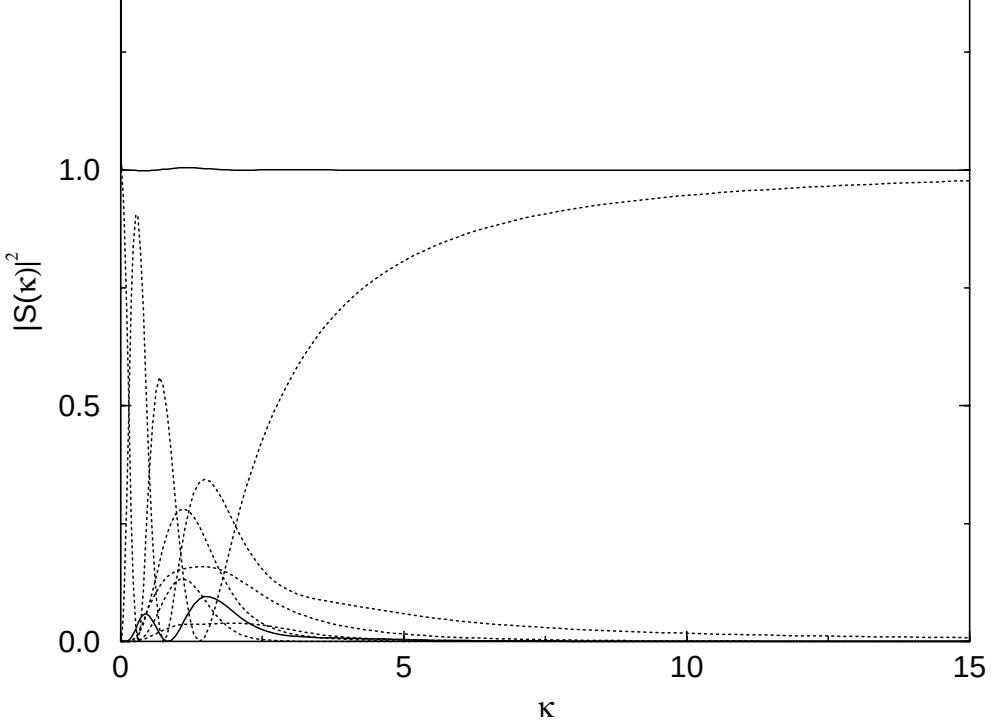

Figure 1:

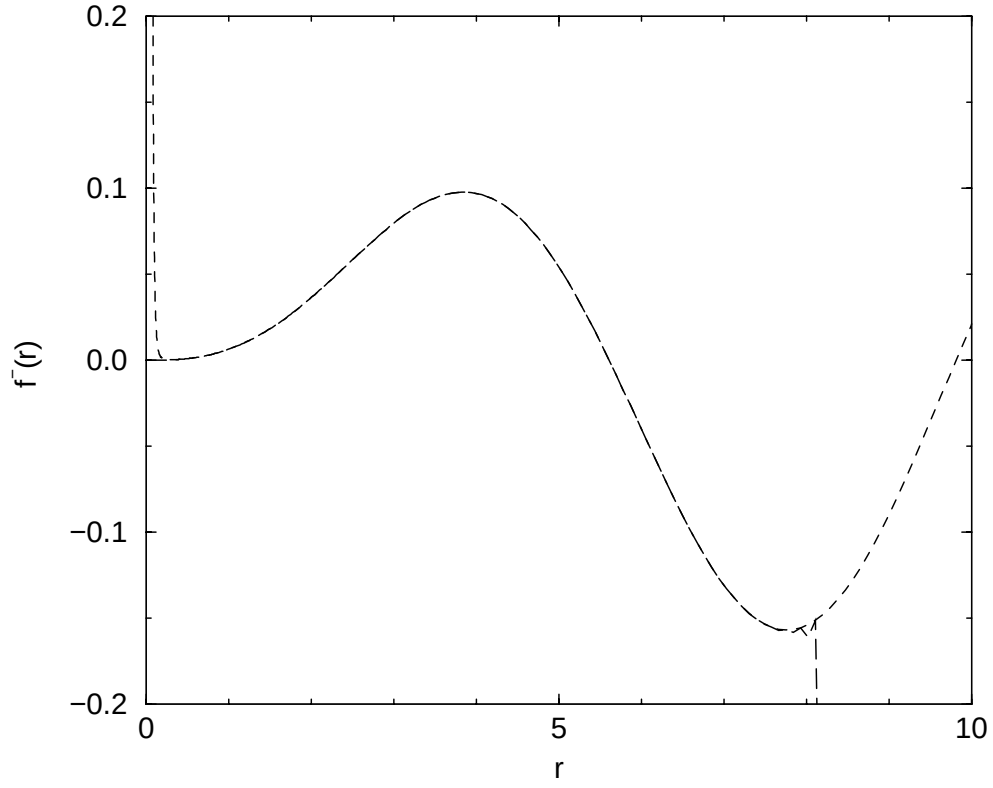

Figure 2:

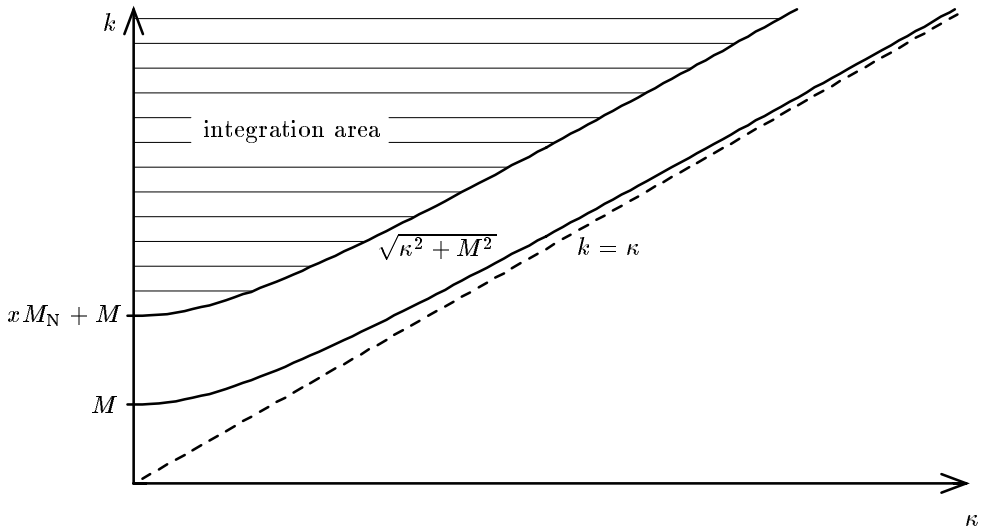

Figure 3:

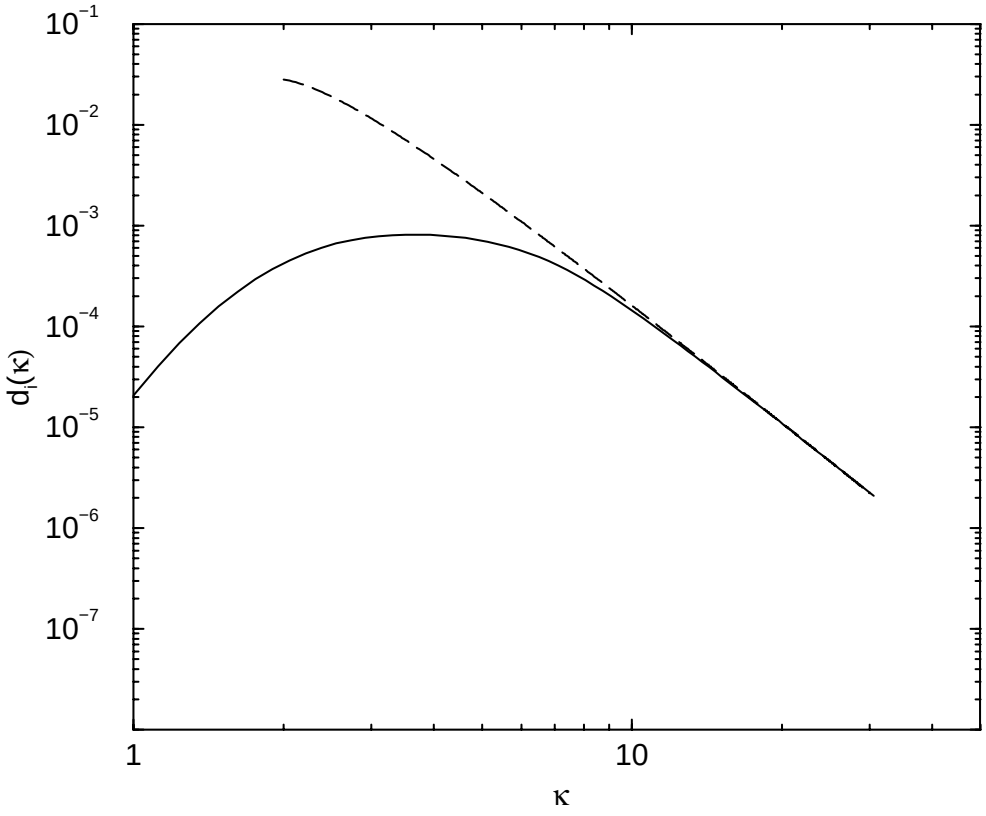

Figure 4:

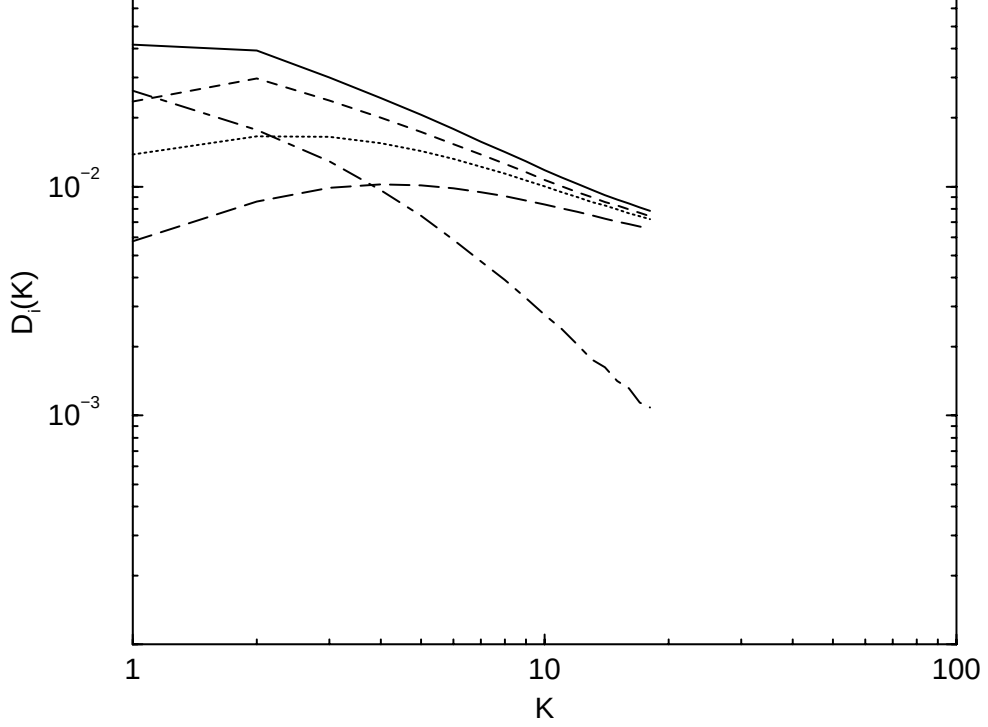

Figure 5:

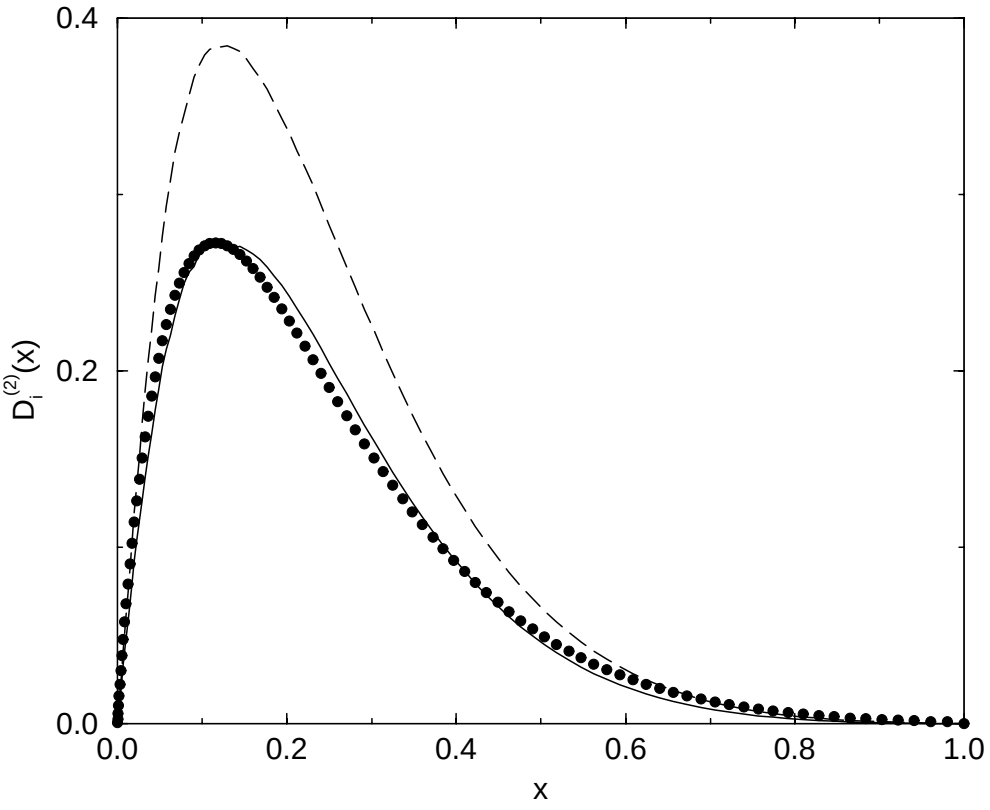

Figure 6:

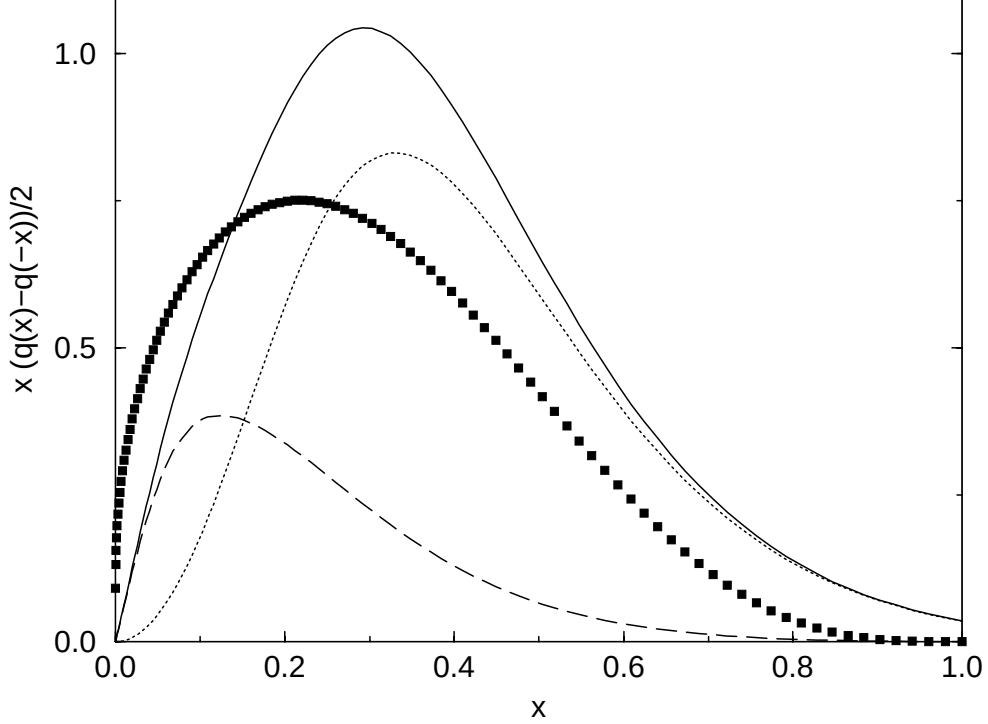

Figure 7:

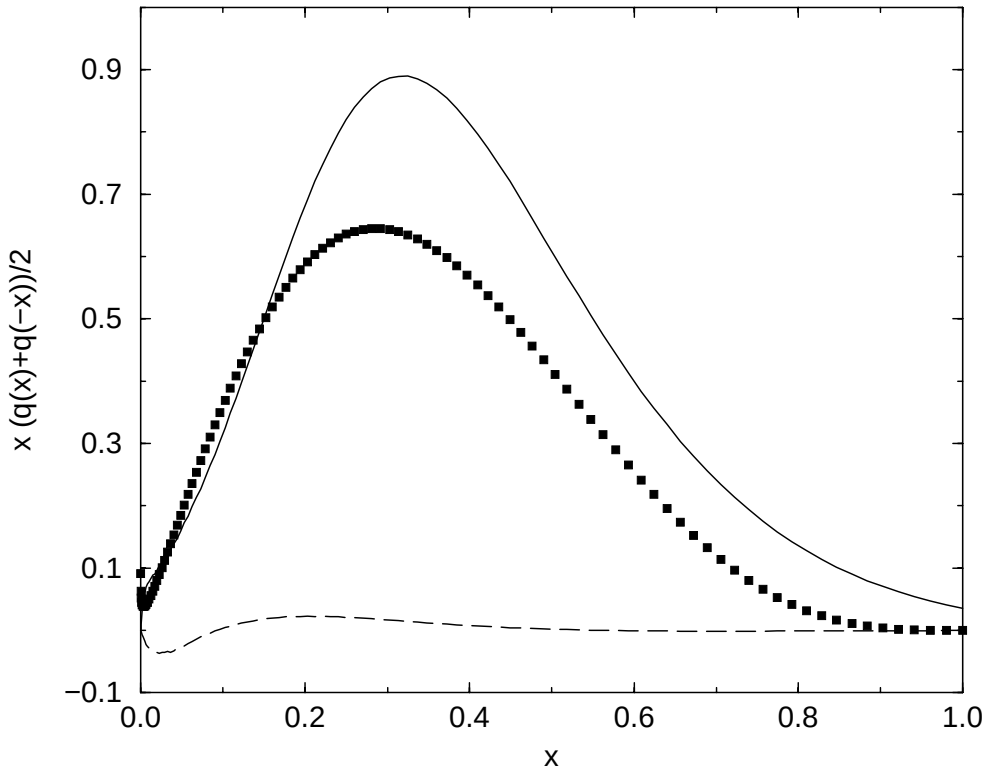

Figure 8: